XI International Conference on Computational Methods in Marine Engineering

Passively pitching blades for wave loading mitigation of horizontal axis tidal turbines

Abel Arredondo-Galeana[1], Gabriel Scarlett[2], Anna Young[3] and Ignazio Maria Viola[4,*]

[1] Department of Naval Architecture, Ocean and Marine Engineering, University of Strathclyde, Glasgow, UK

[2] Mocean Energy Ltd., Edinburgh, EH10 4BY, UK

[3] School of Engineering, Department of Mechanical and Aerospace Engineering, University of Bath,Bath, BA2 7AY, UK

[4] School of Engineering, Institute for Energy Systems University of Edinburgh,Edinburgh, EH10 4BY, UK
[*] I.M.Viola@ed.ac.uk

ABSTRACT

Tidal turbines are subject to large load oscillations due the unsteady marine environment. The variability of loads is detrimental to the fatigue life of tidal turbines and exposes them potentially to premature failure. Passively pitching blades offer the possibility of load alleviation and therefore, long-lasting turbine operation. This can reflect in a reduction in preventive maintenance and operational costs. Nonetheless, the performance of passively pitching blades under realistic flow conditions requires further understanding. In particular, better understanding is needed for tidal turbines that operate in the proximity of ocean waves. In this paper, we explore analytically the loading of a tidal rotor equipped with passively pitching blades, subject to wave loading. We explore low and high amplitude opposing waves acting on the rotor. We find that for small amplitude waves, torque and thrust fluctuations are reduced around the same mean values of a rigid blade tidal turbine. In contrast, for high amplitude waves, although thrust and torque oscillations are also reduced, the mean output power is penalised and power production decreases. These results suggest that passively pitching blade systems might need to be redesigned in environments that include high amplitude waves.

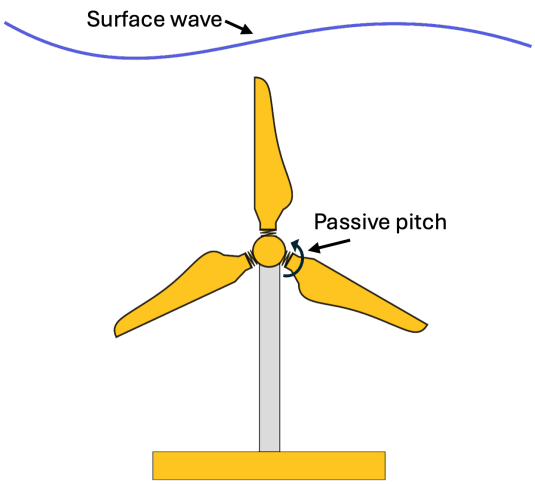

Figure 1: Graphical abstract.

1 Introduction

The tidal sector is growing and recent years have shown great strides towards the route of commercialisation. As an example, in year 2023 in the UK, the contract for difference (CfD) allocation round 5 supported a record number of mega-watt tidal projects. CFDs were awarded to Scottish and Welsh based companies that include MeyGen, Hydrowing, Orbital Marine Power and Magallanes Tidal Energy. In Europe, the capacity of tidal energy that in 2016 was only 3 MW, has been forecasted to grow in year 2025 between 46 to 58 MW, and by 2030 to at least 323 MW Pillet et al. [2025]. Additionally, in the UK, EPSRC government funded projects

such as CoTide and Morphing blades, highlight the interest of different stakeholders in the sector. Although the forecasted capacity might not be met due to current financial and political challenges, the growth of the tidal sector is evident. As capacity grows, the levelised cost of energy (LCOE) reduces and therefore, the future of tidal energy is promising. Nonetheless, the LCOE of tidal turbines needs to be further decreased in order to become more competitive and attract more investment.

Decreasing tidal energy cost is not a trivial task. In particular because tidal turbines face a harsh marine environment and tend to be over engineered to cope with the harsh marine conditions. Structural reliability is a must for tidal turbines and their foundations. In fact, unsteady loading can exacerbate the loading on the blades and in their support structures. In fact, the impact of realistic marine flows on tidal turbines has been the object of recent comprehensive studies [Sequeira and Miller, 2014, Scarlett et al., 2019, Scarlett and Viola, 2020], where it has become clear that unsteady loading on tidal rotors can reduce the operational life of tidal rotors.

Technological developments, such as composite passively bent twist blades, have been introduced to reduce unsteady blade loading [Murray et al., 2018, Porter et al., 2020]. However, the structural response of such blades made with deformable material can be limited to slow frequency fluctuations. Alternatively, active pitch is another feasible load mitigation strategy, but this also has an upper frequency limit due to the inertial effects of the blade [Anderson et al., 1998]. As tidal blades grow in size above 5 m long Lopez Dubon et al. [2024], inertia effects become critical. Localised actuated flaps can respond to higher frequencies than whole-blade control devices due to their smaller size [Young et al., 2016], but such systems may reduce turbine reliability. There is therefore a need to develop reliable load alleviation technology that is responsive to both low and high-frequency fluctuations, to enable tidal developers reduce the cost of energy, without sacrificing reliability.

Over the past decade, passive load alleviation mechanisms of tunable amplitude and frequency response have been proposed [Tully and Viola, 2016, Pisetta et al., 2020]. These concepts have been developed further into generic numerical frameworks of passive pitching systems Ōtomo et al. [2024], Liu et al. [2024], investigating the optimal performance through pitching axis location and finding gust alleviation of up to 75%. In summary, the passively pitching blade concept consists of a blade that is free to pitch around its leading-edge, and that balances the aero/hydrodynamic pitching moment by means of an externally applied constant torque. In an engineering application, the constant torque can be provided via a torsional spring or a constant buoyancy force [Pisetta et al., 2020, Arredondo-Galeana et al., 2021]. Whilst in the natural world, the constant torque can be provided by musculoskeletal forces [Ōtomo et al., 2024, Liu et al., 2024].

A comprehensive review of the numerical assumptions, alongside experimental and numerical validations of the passive pitch system are provided in Viola et al. [2022]. In essence, when an inflow gust occurs, the blade pitches opposite to it, causing a reduction in the angle of attack and therefore, a reduction in loading. For marine renewables, such as tidal turbines, the use of a passive pitching system was explored experimentally in Arredondo-Galeana et al. [2021] through a trailing edge flap, showing that for attached flow conditions, the flap to chord ratio determines the percentage reduction of load alleviation. While Dai et al. [2022] showed with numerical simulations thrust load mitigation in a large scale tidal turbine under shear flow. Subsequently, model scale tests of tidal turbines with passive pitching systems were successfully designed and tested in Gambuzza et al. [2023, 2025]. The tests showed the great prospects into the usefulness of such technology, as a complement to angular velocity control and as a possible substitute to active pitch.

Although total thrust load alleviation under shear is possible, the effectiveness of such technology in realistic ocean conditions remains vastly unexplored. Furthermore it remains unknown, to what extent can passively pitching blades assist in torque peak-to-peak load mitigation. It is known that a pitching blade with a prescribed pitching motion to alleviate thrust loading has a reduced effectiveness in torque loading alleviation under sheared flow [Hu and Willden]. However, the performance of passively pitching systems subject to wave loading has not been comprehensively studied. Hence, in this paper, we explore a turbine with passively pitching blades of adjustable stiffness, subject to low and high amplitude wave loading. We explore to what extent can such system mitigate torque and thrust, while retaining the mean output torque and thrust.

This paper is structured as follows: First, the model scale turbine and numerical modelling considerations are introduced. Then, the model for the passively pitching blade is explained. Then, we compare the torque and

thrust code response for a turbine with rigid blades against experimental data. We compare these results with those of a turbine with variable stiffness passively pitching blades. Lastly the stiffness of the blade is optimised to minimise fluctuations in torque and thrust and results are analysed in different flow conditions.

2 Methodology

2.1 Turbine specifications

The baseline turbine utilised in this study is a 1:15th scale three-bladed prototype tested in FloWave. This turbine was selected because there exist a comprehensive experimental database for numerical code validation. Experimental data for validation is available at the Edinburgh datashare repository [Payne et al., 2017, Draycott et al., 2019]. In particular, Draycott et al. [Draycott et al., 2019] included measurements due to wave and turbulence loading for a rigid bladed turbine. Details of the design and manufacturing of the model-scale turbine are available in Payne et al. [Payne et al., 2017]. The turbine has a rotor diameter of $1.2\mathrm{m}$ and a hub height of $1\mathrm{m}$. The blades are built with NACA 63-8XX profiles. The blade geometry is provided in Payne et al. [Payne et al., 2017]. An schematic of the tidal turbine prototype with rigid and passively pitching blades is shown in Figure 2a and Figure 2b, respectively. The passive pitching blade turbine, depicted in Figure 2b is similar to the concept presented in Gambuzza et al. [2023, 2025], where the blades were designed to passively pitch at the root of the blade.

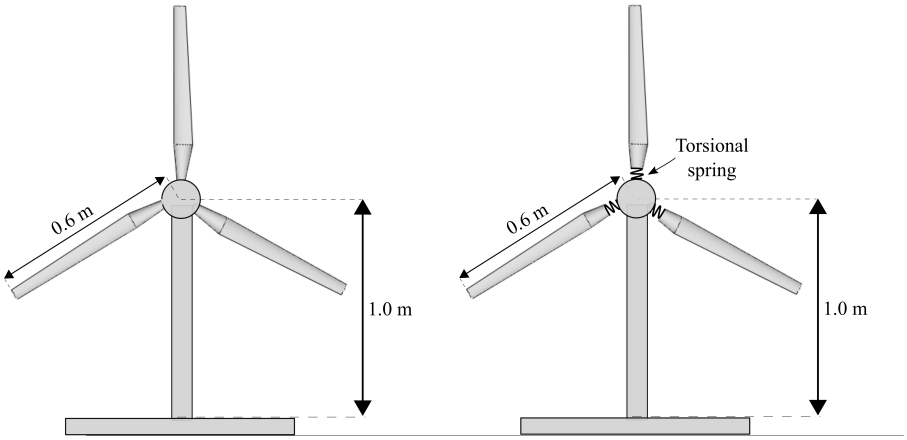

Figure 2: Schematic of FloWave turbine a) with rigid blades and b) with morphing blades.

The loads acting on the turbine are modelled with a blade element momentum (BEM) solver developed by Scarlett et al. [Scarlett et al., 2019, Scarlett and Viola, 2020]. The code is open source and available on the github repository Scarlett [2021]. The open source solver computes the tangential (U_ψ) and the axial (U_x) velocity on different blade sections due to a combination of shear, waves and turbulence. Sheared flow is modelled through a power law, wave loading through Stokes second order wave theory and turbulent flow fluctuations through a von Karman turbulence spectrum. The details of the implementation of these modules are provided in Scarlett and Viola [Scarlett and Viola, 2020].

Once U_ψ and U_x are computed on different sections of the blade considering the combined forcing of shear, waves and turbulence Scarlett et al. [2019], then, the tangential ($a^{'}$) and axial (a) induction factors are computed in the BEM solver. Static NREL-S814 aerofoil data are considered in these iterations. This aerofoil is selected because a large database of empirical dynamic stall coefficients exist for this type of aerofoils. Note that the experimental FloWave turbine is built with the NACA-63-8XX series, however, the NREL profile is retained in the numerical solver to retain the dynamic stall module.

With $a^{'}$, a, U_ψ and U_x, the time histories of the relative velocity (U_{rel}) is computed, such that

$$U_{rel} = \sqrt{[U_\psi(1+a')]^2 + [U_x(1-a)]^2}, \tag{1}$$

and the angle of attack (α) at different blade sections is computed, such that

$$\alpha = \tan^{-1}\left(\frac{U_x(t)(1-a)}{U_\psi(t)(1+a')}\right) - \beta, \tag{2}$$

where β is the sectional twist of the blade. An additional module to modify α from Equation 12 was incorporated, as part of this work. The recomputed α is fed back into the loads module to compute the forces of a turbine with passively pitching blades.

Load time histories for the unsteady lift ($L_{u,i}$) and drag ($D_{u,i}$) of each blade section are computed in the numerical code. Further details of the unsteady load considerations are provided in Scarlett et al. [Scarlett et al., 2019]. A block diagram of the main code for a rigid blade turbine and the incorporation of the morphing blade module is presented in figure 3.

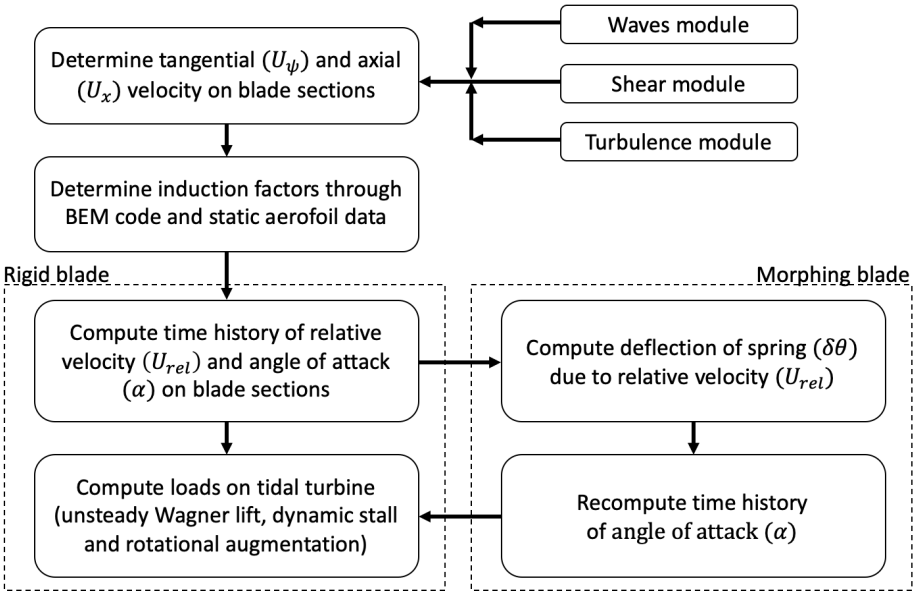

Figure 3: Block diagram of Scarlett's code (available on github) with additional block to recompute the angle of attack on the blade sections due to the deflection of the morphing blade

The torque Q_j and thrust T_j per blade are computed as

$$Q_j = \sum_{i=0}^{n} F_{tan_i} r_i dr \tag{3}$$

and

$$T_j = \sum_{i=0}^{n} F_{t_i} dr, \tag{4}$$

where $F_{tan_i} = L_{u,i}\sin\phi_i - D_{u,i}\cos\phi$ and $F_{t_i} = L_{u,i}\sin\phi_i + D_{u,i}\cos\phi$. The total torque Q and thrust T are obtained by multiplying Q_j and T_j by the total number of blades. Finally, the rotor power for a three bladed turbine is defined as

$$P = \Omega \sum_{j=1}^{3} Q_j, \tag{5}$$

where j is the blade index. The mean power coefficient is computed as

$$C_P = \frac{2P}{\rho A U^3}, \tag{6}$$

where P is the power, ρ is the fluid density, A is the swept area of the rotor and U is the freestream velocity. The mean thrust coefficient is computed as

$$C_T = \frac{2T}{\rho A U^2}, \tag{7}$$

where T is the total thrust.

2.2 Passively pitching blades

Consider the initial position of the blade depicted in Figure 4a in the rotor plane of a tidal turbine. The blade is free to pitch at the leading-edge and has an angle of attack α, twist angle β, inflow angle ϕ, tangential velocity ωR, incident flow velocity U_∞, resultant flow velocity U, lift force L and a torsional spring moment M_k applied to the pitching axis (P.A.).

In Figure 4a, the hydrodynamic pitching moment M_h is equal and opposite to the spring moment, i.e. $M_k = -M_h$. The torsional moment can be defined linearly as

$$M_k = k\theta_0, \tag{8}$$

where θ_0 is the spring preload angle and k is the spring stiffness.

Consider now Figure 4b, where an inflow gust $\delta\alpha$ occurs, while U remains unchanged. Hence, $\delta\alpha$ causes an increase in lift δL and in the pitching moment δM_h. The blade deflects by an angle $\delta\theta$ until the spring and hydrodynamic moments balance each other, such that

$$M_k + \delta M_k = -[M_h + \delta M_h]. \tag{9}$$

For a very flexible spring (very low k) that undergoes a small deflection $\delta\theta$, the left hand side of Equation 9 can be simplified to $M_k = k(\theta_0 \pm \delta\theta) \approx k\theta_0$, because the spring moment is constant. Then, in a first approximation, for the right hand side of Equation (9), we can consider the Reynolds number effect to be small. This implies that L, δL, M_h and δM_h vary linearly with the square of the velocity and with the angle of attack. We therefore rewrite the right hand side term of Equation 9 as

$$-[M_h(\alpha, U^2) + \delta M_h(\Delta\alpha, U^2)], \tag{10}$$

where α is the initial angle of attack and $\Delta\alpha$ is the change in the angle of attack due to $\delta\alpha$ and $\delta\theta$, i.e., $\Delta\alpha = \delta\alpha - \delta\theta$. The new angle of attack on the blade is $\alpha_n = \alpha + \Delta\alpha$ and from Figure 4b, we can define

$$M_h(\alpha, U^2) + \delta M_h(\Delta\alpha, U^2) \approx xL(\alpha, U^2) + x\delta L(\Delta\alpha, U^2), \tag{11}$$

where x is the moment arm of the lift force with respect to the leading-edge of the blade.

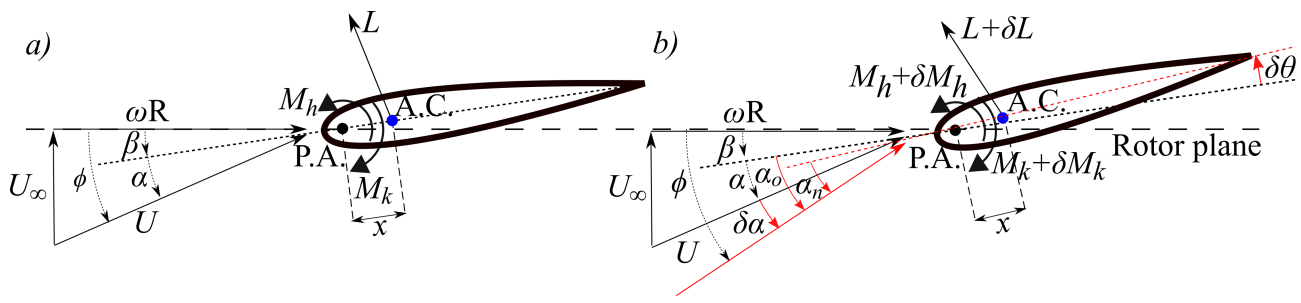

Figure 4: Leading-edge pitching blade in the rotor plane at equilibrium position. The moments M_k and M_h balance each other and act on the pitching axis P.A.

Hence, in order to minimise δL and therefore δM_h, $\Delta\alpha$ needs to be zero. This happens when $\delta\theta = \delta\alpha$, thus preventing any load variation with respect to the initial condition shown in Figure 4a.

From Figure 4b, the angle of attack on the blade after the inflow gust $\delta\alpha$ and the blade deflection $\delta\theta$ is

$$\alpha_n = \phi - \beta - \delta\theta, \tag{12}$$

where ϕ is the inflow angle, β is the twist and $\delta\theta$ is the deflection of the spring from its initial position θ_0. The blade deflection $\delta\theta$ is computed with the moment balance between a torsional spring moment at the root of the blade ($M_h + \delta M_h$), and the sum of the hydrodynamic moments of n-number of blade sections, such that

$$k\theta_0 + k\delta\theta = \sum_{i=1}^{n} \frac{1}{2}\rho U_i^2 c_i^2 C_{LE_i}\delta r, \tag{13}$$

and solving for the deflection of the spring,

$$\delta\theta = \frac{1}{k}\sum_{i=1}^{n} \frac{1}{2}\rho U_i^2 c_i^2 C_{LE_i}\delta r_i - \theta_0, \tag{14}$$

where k is the stiffness of the torsional spring positioned at the root of the blade, i is i-the section of the blade, n is the total number of blade sections, U_i is the sectional relative velocity, c_i is the sectional chord, C_{LE_i} is the leading-edge pitching moment, δr_i is the radial length of each blade section and θ_0 is the initial preload angle of the torsional spring to provide the moment M_k.

In order to solve Equation (14), the leading-edge pitching moment of each blade section is computed as

$$C_{LE_i} = C_{m/4_i} + x\,[C_{L_{u,i}}\cos\alpha_i + C_{D_{u,i}}\sin\alpha_i], \tag{15}$$

where $C_{m/4_i}$ is the quarter chord pitching moment of each blade section, x is the distance from the leading edge to the aerodynamic center of the blade, $C_{L_{u,i}}$ and $C_{D_{u,i}}$ are the unsteady lift and drag sectional coefficients of the blade and α_i is the sectional angle of attack of the blade after the inflow gust and without deflection. Note that Equation (15) is also used in Gambuzza et al. [2025] to compare numerical results to thrust and torque measurements of a tidal turbine equipped with passively pitching blades.

For small angle of attack oscillations, Equation 15 is linearised, such that

$$C_{LE_i} = m\alpha_{n_i} + b. \tag{16}$$

By combining Equation 16 and Equation 14 into Equation 12, the new sectional angle of attack α_{n_i}, after blade deflection, is computed. Note that the preload angle θ_0 in Equation 14 is computed by utilising the mean flow velocity $\overline{U}$ and the mean flow angle $\overline{\alpha}$ at equilibrium conditions (Figure 4a), with

$$k\theta_0 = \sum_{i=1}^{n} \frac{1}{2}\rho \overline{U}^2 c_i^2 C_{LE}(\overline{\alpha})\delta r. \tag{17}$$

3 Results

3.1 C_P and C_T curves at uniform flow conditions

The hydrodynamic BEM code is benchmarked versus experimental measurements of tidal turbine prototype with rigid blades tested in FlowWave [Draycott et al., 2019]. We assume a $1/15^{\text{th}}$ power law, which corresponds to the shear velocity profile measured in FloWave [Draycott et al., 2019]. The verification is carried out because the original numerical code was implemented with blade data of a full scale turbine Scarlett et al. [2019], Scarlett and Viola [2020]. Hence, in this work we modify the turbine and blade dimensions to match the turbine scale model used for experimental testing in FlowWave [Payne et al., 2017, Draycott et al., 2019, Gambuzza et al., 2023, 2025].

Average C_P and C_T values versus different tip speed ratios (λ) are plotted in Figure 5a and 5b, respectively. Experimental measurements are plotted with circular black markers. Numerical simulations with rigid blades are plotted with red markers. While simulation results with passively pitching blades are plotted with blue markers. In general, a satisfactory experimental and numerical agreement is obtained for both C_P and C_T in both Figure 5a and 5b. Nonetheless, in Figure 5a, the numerical simulations slightly over estimate the mean power coefficient C_P when $\lambda \geq 4.5$. The discrepancy could be due to the dynamic stall assumptions used in the numerical code, which estimate high lift and drag values when $\lambda \geq 7$.

Another important observation is that Figure 5a shows that the average C_P and C_T values do not change between rigid and passively pitching blades. These results confirm previous observations demonstrated analytically, experimentally and numerically [Pisetta et al., 2020, Arredondo-Galeana et al., 2021, Dai et al., 2022]. Hence, passively pitching blades are not detrimental to performance in uniform shear flow. We recall that this occurs because the mean angle of attack of the passively pitching blade is the same as that of the rigid blade, due to the spring moment balancing the mean hydrostatic moment, as stated in Equation (9).

In terms of the mean thrust coefficient C_T, Figure 5b shows than when $\lambda \leq 4.5$, the simulated data is slightly over predicted. Nonetheless discrepancies are not severe. In particular, the experimental uncertainties reported in Draycott et al. [Draycott et al., 2019] include the range of values of the simulated data. In both Figure 5 and Figure 5, the numerical C_P and C_T values are at best agreement at the optimum tip speed ratio $\lambda = 7$. Therefore, this is the λ where the performance of the passively pitching blade is analysed in the rest of the manuscript.

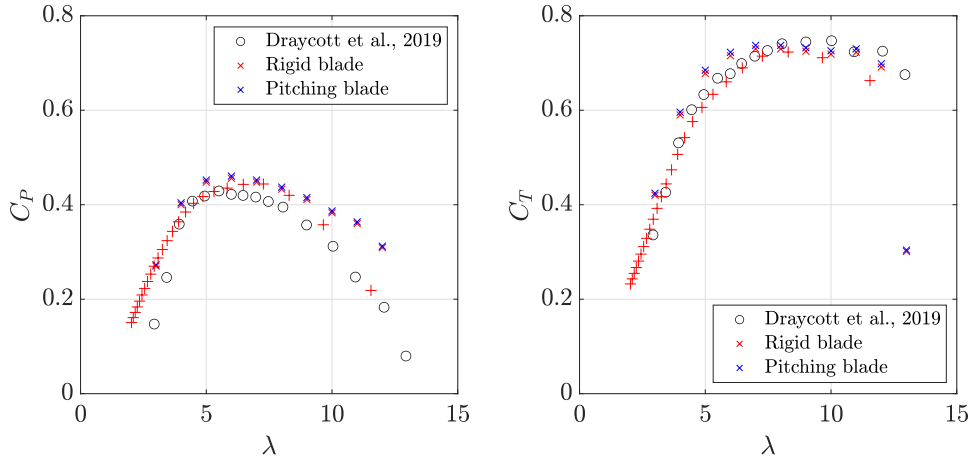

Figure 5: a) C_P and b) C_T curves at uniform sheared flow by Draycott et al. (circle), simulated with rigid blades (red cross), with passively pitching blades (blue cross) and rigid blades in open source solver (red marker)

3.2 Instantaneous torque and thrust analysis

In this section, we assess now the performance of the turbine equipped with passively pitching blades subject to wave loading conditions. Two conditions are tested: 1) low height opposite waves ($H = 0.1$ m and $T = 2.5$ s) and 2) big height opposite waves ($H = 0.4$ m and $T = 3.4$ s). Opposite shear and waves have been shown to combine to form more sinusoidal type of waves Chen and Zou [2019]. Hence, these are the types of flow conditions selected in this study.

3.2.1 Case 1: Low amplitude waves

The wave conditions for the first case, referred to as low wave amplitude case, consists of opposing waves at $T_s = 2.5\,\mathrm{s}$ and $H = 0.1\,\mathrm{m}$. Isotropic turbulence and turbulence intensity of $I = 8\%$ are considered. Figure 6a and Figure 6b shows the instantaneous torque (Q) and thrust (T) of a rigid blade turbine in FlowWave [Draycott et al., 2019], compared to the simulated values of a turbine equipped with rigid and passively pitching blades. The passively pitching blades are implemented with two different spring stiffness. Namely, low ($k = 0.15$) and intermediate ($k = 0.40$) stiffness.

Figure 6a shows that torque loading remains fairly similar between the experimental (yellow solid line) and all of the simulated cases. The latter are plotted in red, black and blue for the rigid, low stiffness and intermediate stiffness cases, respectively. In contrast, Figure 6b shows that thrust oscillations are visibly flattened with a low stiffness spring ($k = 0.15$), as shown by the black solid line.

A reduction in peak to peak thrust loading as indicated in Figure 6b with the low stiffness spring is beneficial for structural integrity. Given that it reduces fatigue loading and the impact of cyclic loading due to waves Arredondo-Galeana et al. [2023b,a]. Secondly, as indicated in Figure 6a, it is desirable that the turbine equipped with passively pitching blades retains the same torque and power output profile than the rigid blade counterpart. Therefore, the performance of the low stiffness passively pitching blades in the low wave amplitude case is ideal.

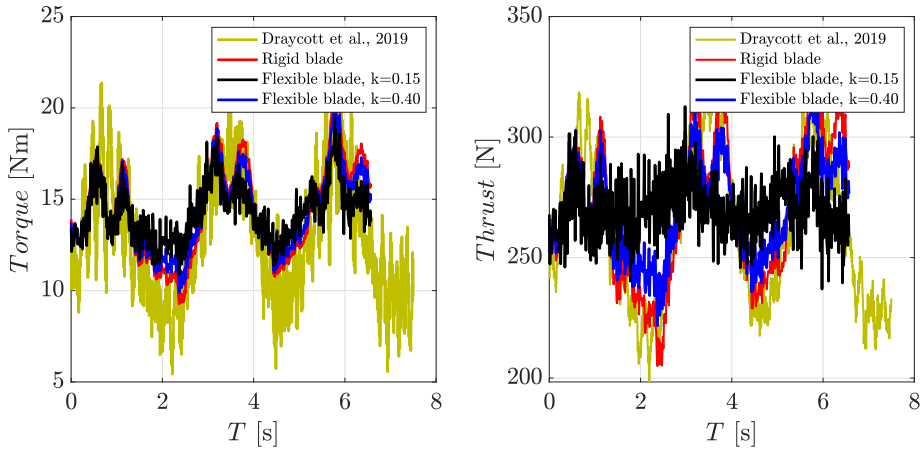

Figure 6: a) Torque and b)thrust instantaneous curves for opposing waves at $T_s = 2.5\,\mathrm{s}$ and $H = 0.1\,\mathrm{m}$ measured by Draycott et al. 2019 (blue), simulated (red), with optimal morphing blades (black), suboptimal morphing blades (dark blue)

3.2.2 Case 2: High amplitude waves

The second test case consists of opposing waves at $T_s = 3.4\,\mathrm{s}$ and $H = 0.4\,\mathrm{m}$. Isotropic turbulence and turbulence intensity $I = 8\%$ are considered. Results are presented in Figure 6a and Figure 6b for instantaneous torque and thrust, respectively.

For this case, as indicated in Figure 6a, it can be seen with the black solid lines, that the peak torque values of a turbine equipped with low stiffness passively pitching blades drops in comparison to the more rigid blade counterparts (yellow, red and blue solid lines). Consequently, the mean torque value of the low stiffness blade turbine decreases too, in comparison to the mean torque value of a rigid blade turbine. In contrast, Figure 6b shows that the low stiffness spring blade turbine provides a similar mean thrust value as that of the rigid blade turbine counterparts, and importantly, it still provides thrust load alleviation, as in the previous case of low amplitude waves.

In conclusion, for the high wave amplitude case, it can be said that for the high amplitude wave case, thrust and torque peak load alleviation comes at a penalty of mean power loss. As indicated in Arredondo-Galeana et al. [2024], for a foil-energy device equipped with passively pitching blades in waves, a possible reason for a drop in power performance is that the linearisation assumption used in Equation (16) is not applicable in the high wave amplitude regime. However, the cause of drop in performance with a tidal rotor is still under investigation by the authors of this paper.

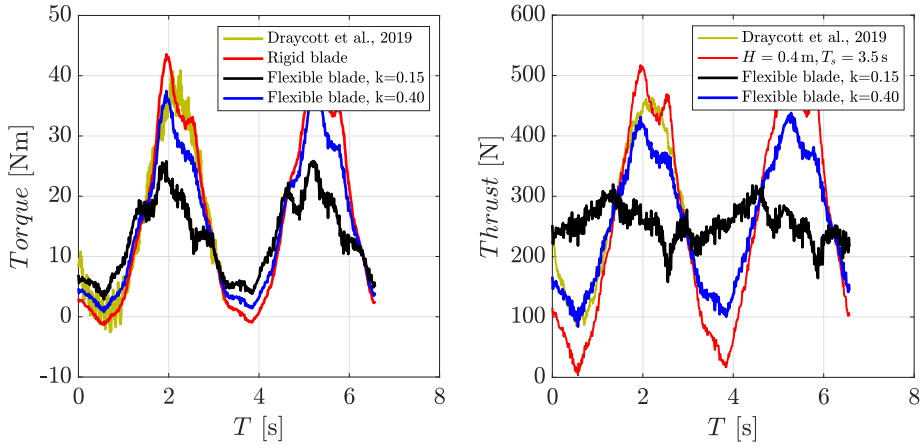

Figure 7: a) Torque and b)thrust for opposing waves at $T_s = 3.4\,\mathrm{s}$ and $H = 0.4\,\mathrm{m}$ measured by Draycott et al. 2019 (blue), simulated (red), with optimal morphing blades (black), suboptimal morphing blades (dark blue)

To visualise better the mean performance of the turbine in the low and high wave amplitude cases, the mean torque ($\overline{Q}$) and mean thrust ($\overline{T}$) are studied in this section. Figure 8a and Figure 8b show $\overline{Q}$ and $\overline{T}$, respectively, for case 1 - low amplitude wave - and case 2 - high amplitude wave.

Figure 8a and Figure 8b show $\overline{Q}$ and $\overline{T}$, respectively, for the experiments in FlowWave [Draycott et al., 2019], and numerically rigid, intermediate ($k = 0.40$) and low stiffness ($k = 0.15$) blades, as labeled in the horizontal axes of the figures. Case 1 - low amplitude waves - is plotted with slim gray bars at the front of the figures. While Case 2 - high amplitude waves - is plotted with thicker black bars, at the background of the figures.

Figure 8a shows that for Case 1 (gray bars), $\overline{Q}$ remains relatively stable for all of the presented scenarios, i.e. experiments (FloWave), rigid and passively pitching blades of intermediate and low stiffness. The same can be observed in terms of $\overline{T}$ in Figure 8b for Case 1. In contrast, Figure 8a shows that for Case 2 (black bars), high amplitude waves, $\overline{Q}$ drops with very low stiffness passively pitching blades. In terms of $\overline{T}$, Figure 8b, the black bars show that $\overline{T}$ remains constant for all of the scenarios presented in the Figure.

Results presented in this section confirm that a low stiffness passively pitching blade turbine retains the same mean torque and mean thrust, as that of a rigid blade turbine, in slow amplitude waves. In contrast, high ampli-

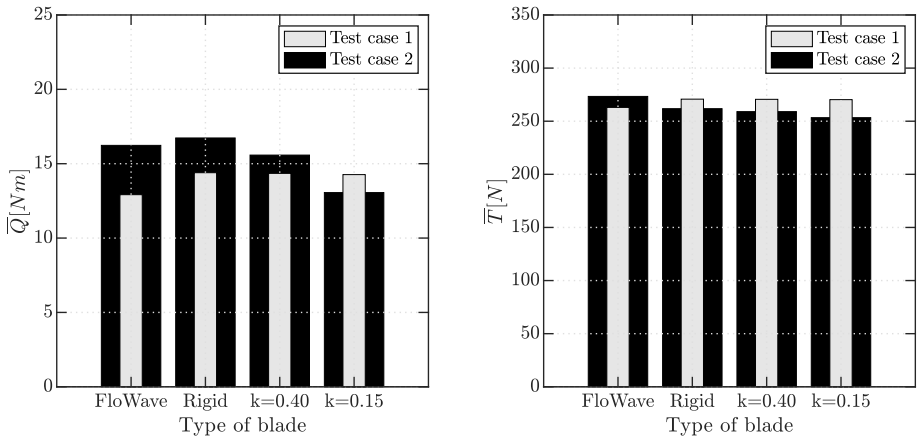

Figure 8: a) Mean torque and thrust for different blades (FloWave, Rigid, $k = 0.40$, $k = 0.15$) at two flow test cases (gray and black)

tude waves pose performance challenges in terms of power performance. Nonetheless, thrust load alleviation is still feasible. Although the deficit in power at high amplitude waves could be due large angle of attack oscillations and due to numerical limitations of this work. In real systems, rotational speed control combined with passively pitching blades, can be implemented to reduce the amplitude of the angle of attack oscillations, and therefore, retain power performance **?**Gambuzza et al. [2025].

3.3 Blade stiffness optimisation versus peak loading mitigation ratio and mean output ratio

In this section, the stiffness of the passively pitching spring is optimised versus two objectives. The first objective is set to minimise the ratio of peak to peak torque and thrust fluctuations between passively pitching and rigid blades. The ratios are defined as $\Delta Q_k/\Delta Q_r$ and $\Delta T_k/\Delta T_r$, respectively. Where ΔQ_k and ΔT_k are the peak to peak fluctuations of torque and thrust of the turbine with passively pitching blades, respectively. While ΔQ_r and ΔT_r are the peak to peak fluctuations of torque and thrust of the turbine with rigid blades, respectively. Low $\Delta Q_k/\Delta Q_r$ and $\Delta T_k/\Delta T_r$ values would ensure minimal fluctuations around the mean torque and thrust values, respectively. Note that a reduction in both torque and thrust fluctuations are desirable from both power and structural integrity perspectives.

The second objectives is to maintain the mean torque and thrust between rigid and passively pitching blade turbines equal. We define the ratios $\overline{Q_k}/\overline{Q_r} = 1$ and $\overline{T_k}/\overline{T_r} = 1$. Where $\overline{Q_k}$ and $\overline{T_k}$ are the mean torque and thrust of the turbine with passively pitching blades, respectively. While $\overline{Q_r}$ and $\overline{T_r}$ are the mean torque and thrust of the turbine with rigid blades, respectively. The condition where $\overline{Q_k}/\overline{Q_r} = 1$ and $\overline{T_k}/\overline{T_r} = 1$ ensures that the passively pitching blades are not detrimental to turbine performance.

The described ratios are computed for the two different wave cases analysed in this work, namely, the low amplitude ($H = 0.1\,\mathrm{m}$) and high amplitude waves ($H = 0.4\,\mathrm{m}$). In Figure 9a, we show the power performance, with the $\Delta Q_k/\Delta Q_r$ and the $\overline{Q_k}/\overline{Q_r}$ ratios plotted for a range of different spring stiffness ($0.0 \leq k \leq 0.5$). Figure 9b shows the thrust performance, with the $\Delta T_k/\Delta T_r$ and the $\overline{T_k}/\overline{T_r}$ ratios, also plotted as a function of different spring stiffness ($0.0 \leq k \leq 0.5$).

Figure 9a shows that in terms of mean torque ratios (black lines), at low amplitude waves (solid black line), the mean torque of the passively rigid blade turbine remains the same as that of the rigid blade counter part ($\overline{Q_k}/\overline{Q_r} \approx 1$), independently of the spring stiffness (k). In contrast, for higher amplitude waves (dotted black line), the mean torque value is lower than that of the rigid blade counter part ($\overline{Q_k}/\overline{Q_r} < 1$). In particular, $\overline{Q_k}/\overline{Q_r} \approx 0.65$ at a spring stiffness of $k = 0.1$.

In terms of torque oscillations, the red lines of Figure 9a show that for both low (solid red line) and high amplitude waves (dotted red line), the peak to peak torque fluctuations of the passively pitching blade turbine

are always lower than those of the rigid blade turbine ($\Delta Q_k/\Delta Q_r < 1$). In particular, the peak to peak values drop with lower spring stiffness. Note that the drop in $\Delta Q_k/\Delta Q_r$ for the passively pitching blade turbine is more significant for high amplitude waves, as depicted by the red dotted line in Figure 9a.

With respect to thrust loading, Figure 9b shows that $\overline{T_k}/\overline{T_r} \approx 1$, independently from k, for both low and high amplitude waves, as depicted with the solid an dotted black lines, respectively. In terms of $\Delta T_k/\Delta T_r$, Figure 9b shows that passively pitching blades reduce peak thrust loading in both low and high amplitude waves, as depicted with the solid and dotted red lines, respectively. As indicated by the red lines in Figure 9b, the thrust load alleviation changes with blade stiffness for both low and high amplitude waves. In fact, there is an optimum value at which the drop in peak to peak thrust loading can drop by approximately 40% at low amplitude waves, and 70% at high amplitude waves. Hence, from a structural perspective and cyclic fatigue loading Arredondo-Galeana et al. [2023b], optimally tuned passively pitching blades offer a superior performance.

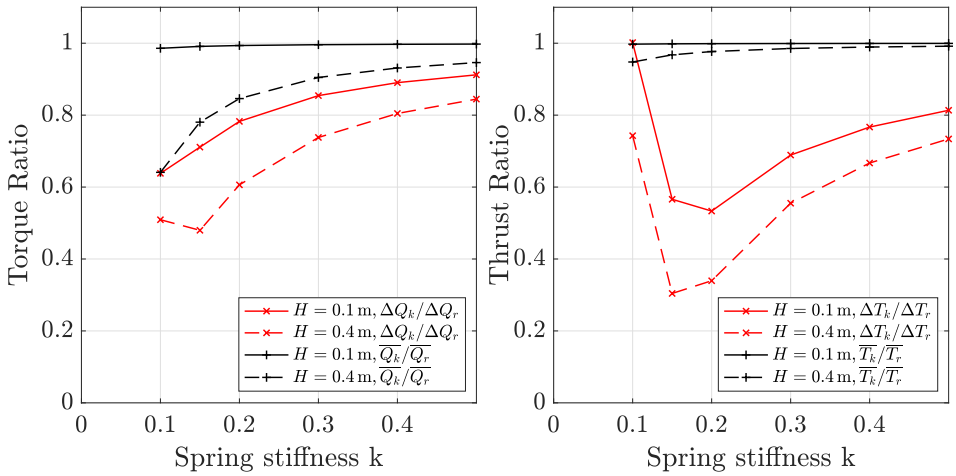

Figure 9: Spring stiffness optimisation for torque Q and thrust T for the two tested wave cases

4 Conclusions

In this work, we present a theoretical study on the performance of passively pitching blades on tidal turbines that are subject to wave loading. Two cases are studied: one with low amplitude waves, and one with high amplitude waves. Both waves are opposed to the direction of the shear current. Note that although great progress has been made on the understanding of the performance of passively pitching blades for torque and thrust control in tidal turbines, there is a lack of understanding of these systems subject to wave loading. Hence, herein lies the novelty of this study. We summarise next the main conclusions of this study:

1. Wave loading is an important factor that contributes to cyclic loading in tidal turbines. Hence, it must be considered to assess fatigue life and structural integrity of tidal turbines.

2. Passively pitching blades can provide load alleviation because they can flex in response to external wave gusts, reducing the the angle of attack on the blades, and therefore minimising load oscillations.

3. Passively pitching blade turbines operating in low amplitude opposing waves have similar performance than morphing blades operating in pure shear. That is, thrust load alleviation around the mean thrust value, while retaining mean output power similar to a rigid blade turbine.

4. Passively pitching blade turbines operating in high amplitude opposing waves still provide thrust load oscillations alleviation, while retaining mean thrust levels as those of a rigid blade turbine. However,

the mean torque value is penalised. This is possibly due to the hydrodynamic moment not being linear anymore due to large angle of attack oscillations.

5. Combination of active control techniques, such as optimal speed control could help in alleviating the limitations encountered in high amplitude waves.

Therefore, passively pitching blades are an appealing alternative for load alleviation of tidal turbine subject to wave loading. In particular, for low amplitude waves, mean power performance is not affected. For high amplitude waves, mean power performance drops, nonetheless, the structural reliability of the turbine is protected, making passive pitch a worthy fatigue life extension system.

Acknowledgments

This work was supported by the UK Engineering and Physical Sciences Research Council through the grant 'Morphing-Blades: New-Concept Turbine Blades for Unsteady Load Mitigation' [EP/V0094 43/1].

References

C. G. Anderson, J. . Richon, and T. J. Campbell. An aerodynamic moment-controlled surface for gust load alleviation on wind turbine rotors. *IEEE Transactions on Control Systems Technology*, 6(5):577–595, Sep. 1998. ISSN 2374-0159. doi: 10.1109/87.709493.

Abel Arredondo-Galeana, Anna M. Young, Amanda S.M. Smyth, and Ignazio Maria Viola. Unsteady load mitigation through a passive trailing-edge flap. *Journal of Fluids and Structures*, 106: 103352, 2021. ISSN 0889-9746. doi: https://doi.org/10.1016/j.jfluidstructs.2021.103352. URL https://www.sciencedirect.com/science/article/pii/S0889974621001353.

Abel Arredondo-Galeana, Saishuai Dai, Yongqiang Chen, Xiantao Zhang, and Feargal Brennan. Understanding the force motion trade off of rigid and hinged floating platforms for marine renewables. 15:1–10, September 2023a. doi: 10.36688/ewtec-2023-389. URL https://ewtec.org/ewtec-2023/. The 15th European Wave and Tidal Energy Conference ; Conference date: 03-09-2023 Through 07-09-2023.

Abel Arredondo-Galeana, Paul Lamont-Kane, Weichao Shi, Matt Folley, and Feargal Brennan. A probabilistic framework for fatigue damage of lift based wave energy converters. 15:1–10, September 2023b. doi: 10.36688/ewtec-2023-393. URL https://ewtec.org/ewtec-2023/. The 15th European Wave and Tidal Energy Conference ; Conference date: 03-09-2023 Through 07-09-2023.

Abel Arredondo-Galeana, Andrei Ermakov, Weichao Shi, John V. Ringwood, and Feargal Brennan. Optimal control of wave cycloidal rotors with passively morphing foils: An analytical and numerical study. *Marine Structures*, 95:103597, 2024. ISSN 0951-8339. doi: https://doi.org/10.1016/j.marstruc.2024.103597. URL https://www.sciencedirect.com/science/article/pii/S095183392400025X.

Haifei Chen and Qingping Zou. Effects of following and opposing vertical current shear on nonlinear wave interactions. *Applied Ocean Research*, 89:23–35, 2019. ISSN 0141-1187. doi: https://doi.org/10.1016/j.apor.2019.04.001. URL https://www.sciencedirect.com/science/article/pii/S0141118718307065.

Weidong Dai, Riccardo Broglia, and Ignazio Maria Viola. Mitigation of rotor thrust fluctuations through passive pitch. *Journal of Fluids and Structures*, 112:103599, 2022. ISSN 0889-9746. doi: https://doi.org/10.1016/j.jfluidstructs.2022.103599. URL https://www.sciencedirect.com/science/article/pii/S0889974622000573.

S. Draycott, G. Payne, J. Steynor, A. Nambiar, B. Sellar, and V. Venugopal. An experimental investigation into non-linear wave loading on horizontal axis tidal turbines. *Journal of Fluids and Structures*, 84:199 – 217, 2019. ISSN 0889-9746. doi: https://doi.org/10.1016/j.jfluidstructs.2018.11.004.

Stefano Gambuzza, Gabriele Pisetta, Thomas Davey, Jeffrey Steynor, and Ignazio Maria Viola. Model-scale experiments of passive pitch control for tidal turbines. *Renewable Energy*, 205: 10–29, 2023. ISSN 0960-1481. doi: https://doi.org/10.1016/j.renene.2023.01.051. URL https://www.sciencedirect.com/science/article/pii/S0960148123000605.

Stefano Gambuzza, Puja Sunil, Mario Felli, Anna M. Young, Riccardo Broglia, Edward D. McCarthy, and Ignazio Maria Viola. Power and thrust control by passive pitch for tidal turbines. *Renewable Energy*, 239:121921, 2025. ISSN 0960-1481. doi: https://doi.org/10.1016/j.renene.2024.121921. URL https://www.sciencedirect.com/science/article/pii/S096014812401989X.

J. Hu and R.H.J. Willden. Unsteady load relief of an axial flow tidal turbine in sheared flow by individual pitch control. In *5th Oxford Tidal Energy Workshop*.

Yabin Liu, Riccardo Broglia, Anna M. Young, Edward D. McCarthy, and Ignazio Maria Viola. Unsteady load mitigation through passive pitch. *Journal of Fluids and Structures*, 131: 104216, 2024. ISSN 0889-9746. doi: https://doi.org/10.1016/j.jfluidstructs.2024.104216. URL https://www.sciencedirect.com/science/article/pii/S0889974624001518.

Sergio Lopez Dubon, Christopher Vogel, David Garcia Cava, Fergus Cuthill, Edward D. McCarthy, and Conchur M. Ó Bradaigh. A full-scale tidal blade fatigue test using the fastblade facility. *Renewable Energy*, 228:120653, 2024. ISSN 0960-1481. doi: https://doi.org/10.1016/j.renene.2024.120653. URL https://www.sciencedirect.com/science/article/pii/S0960148124007213.

Robynne E. Murray, Stephanie Ordonez-Sanchez, Kate E. Porter, Darrel A. Doman, Michael J. Pegg, and Cameron M. Johnstone. Towing tank testing of passively adaptive composite tidal turbine blades and comparison to design tool. *Renewable Energy*, 116:202–214, 2018. ISSN 0960-1481. doi: https://doi.org/10.1016/j.renene.2017.09.062. URL https://www.sciencedirect.com/science/article/pii/S0960148117309254.

Grégory S. Payne, Tim Stallard, and Rodrigo Martinez. Design and manufacture of a bed supported tidal turbine model for blade and shaft load measurement in turbulent flow and waves. *Renewable Energy*, 107: 312 – 326, 2017. ISSN 0960-1481. doi: https://doi.org/10.1016/j.renene.2017.01.068.

AC Pillet, B Lehner, S Stark, and H van der Zant. Mapping out the scenarios of ocean energy scale-up based on the development of offshore wind [version 2; peer review: 5 approved with reservations]. *Open Research Europe*, 3(102), 2025. doi: 10.12688/openreseurope.15906.2.

Gabriele Pisetta, Robin Le Mestre, and Ignazio Maria Viola. Passive load control of a tidal turbine. *Renewable Energy*, 146:843 – 855, 2020. ISSN 0960-1481. doi: https://doi.org/10.1016/j.renene.2019.06.153.

Kate E. Porter, Stephanie E. Ordonez-Sanchez, Robynne E. Murray, Matthew Allmark, Cameron M. Johnstone, Tim O'Doherty, Allan Mason-Jones, Darrel A. Doman, and Michael J. Pegg. Flume testing of passively adaptive composite tidal turbine blades under combined wave and current loading. *Journal of Fluids and Structures*, 93:102825, 2020. ISSN 0889-9746. doi: https://doi.org/10.1016/j.jfluidstructs.2019.102825.

Gabriel Thomas Scarlett. transtide: Tidal turbine unsteady load model. https://github.com/gabscarlett/transTide, 2021. Accessed: 2025-05-26.

Gabriel Thomas Scarlett and Ignazio Maria Viola. Unsteady hydrodynamics of tidal turbine blades. *Renewable Energy*, 146:843 – 855, 2020. ISSN 0960-1481. doi: https://doi.org/10.1016/j.renene.2019.06.153.

Gabriel Thomas Scarlett, Brian Sellar, Ton van den Bremer, and Ignazio Maria Viola. Unsteady hydrodynamics of a full-scale tidal turbine operating in large wave conditions. *Renewable Energy*, 143:199 – 213, 2019. ISSN 0960-1481. doi: https://doi.org/10.1016/j.renene.2019.04.123.

C. L. Sequeira and R. J. Miller. Unsteady gust response of tidal stream turbines. In *2014 Oceans - St. John's*, pages 1–10, Sep. 2014. doi: 10.1109/OCEANS.2014.7003026.

Susan Tully and Ignazio Maria Viola. Reducing the wave induced loading of tidal turbine blades through the use of a flexible blade. In *16th International Symposium on Transport Phenomena and Dynamics of Rotating Machinery (ISROMAC 2016)*, Honolulu, United States, April 2016.

Ignazio Maria Viola, Gabriele Pisetta, Weidong Dai, Abel Arredondo-Galeana, Anna Young, and Amanda Smyth. Morphing blades: Theory and proof of principles. *International Marine Energy Journal*, 5(2):183–193, Sep. 2022. doi: 10.36688/imej.5.183-193. URL https://marineenergyjournal.org/imej/article/view/126.

Anna M. Young, Judith R. Farman, and Robert J. Miller. Load alleviation technology for extending life in tidal turbines. In C. Guedes Soares, editor, *Progress in Renewable Energies Offshore - Proceedings of 2nd International Conference on Renewable Energies Offshore, RENEW 2016*, pages 521–530, USA United States, 10 2016. CRC Press. ISBN 9781138626270.

Shuji Ōtomo, Stefano Gambuzza, Yabin Liu, Anna Young, Riccardo Broglia, Edward McCarthy, and Ignazio Maria Viola. A general framework for the design of efficient passive pitch systems. *Physics of Fluids*, 36(6), June 2024. ISSN 1070-6631. doi: 10.1063/5.0212626.